Romanian Journal of Earth Sciences 85 (2011) 19-34

A reconnaissance study on selected intrusive bodies south of Panzhihua, Sichuan Province, South-West China: petrogenetic and metallogenetic significance

Marian MUNTEANU[1,2,*], Yong YAO[1,3], Mihaela CIOACĂ[2], Gordon CHUNNETT[1], Yaonan LUO[4]

[1]School of Geosciences, University of the Witwatersrand, Johannesburg, South Africa, [2]Geological Institute of Romania, Bucharest, Romania, [3]Department of Geology, Rhodes University, Grahamstown, South Africa, [4]Sichuan Bureau of Geology and Mineral Resources, Chengdu, China

Abstract: This paper provides petrographic and geochemical data (major and trace elements) on selected Permian intrusions south of Panzhihua municipality: Luobodi (gabbro hosting Fe-Ti-V oxide ore), Jizicheng (dunitic peridotite and olivine pyroxenite ± gabbro), Gongshanqing (gabbro and peridotite hosting PGE mineralization), one gabbro body and two picrite dikes intruded in the southern part of the Datian Proterozoic complex. These intrusions are genetically related to the Permian Emeishan large igneous province. The attempt to find a geochemical correlation between the investigated intrusions and the high-Ti or low-Ti Emeishan basalts yielded ambiguous results. Most of the rocks have Ti/Y > 500, similar to the high-Ti basalts, while Zr/Nb and La/Yb ratios are similar to those of the low-Ti Emeishan basalts. The ultramafic rocks in the Gongshanqing and Jizicheng intrusions have Cu/Zr ≥ 1 and Cu/Pd ratios within the mantle range (1000-10000), which suggests their genesis from magmas fertile in chalcophile elements. The formation of the Gongshanqing and Jizicheng intrusions in magmatic conduits is inferred.

***Keywords*:** mafic, ultramafic, Emeishan large igneous province, Permian, Panxi rift, China

1. Introduction

The western part of the Yangtze craton is characterized by the presence of a zone of crustal extension, known in the Chinese literature as the Panxi zone or the Panxi rift (Fig. 1A), named from the two municipalities of Panzhihua and Xichang (Fig. 1B). The Panxi rift is located within the Emeishan large igneous province (Xu et al., 2001), made up of the Emeishan basalts, ca. 260 Ma in age (Zhou et al., 2002a), and numerous intrusions cropping out within the Panxi rift. The Emeishan basalts were divided in two geochemical types of low-Ti and high-Ti compositions (Xu et al., 2001; Xiao et al., 2004; Xu et al., 2004; Ali et al., 2005; Zhou et al., 2008). The low-Ti basalts have TiO_2<2.5% and Ti/Y<500, while high-Ti basalts are characterized by Ti/Y>500 and TiO_2>2.5% (Xu et al., 2001).

Most intrusions of the Emeishan large igneous province crop out within the Panxi rift, and contain various rock types (peridotite, pyroxenite, gabbro, syenite, alkaline granite). The Panxi rift is economically important as it contains several ore deposits hosted in intrusive bodies. These deposits are of two main types: giant-scale Fe-Ti-V oxide deposits (Panzhihua, Hongge, Baima, Taihe) and smaller Ni-Cu(-PGE) sulfide deposits (e.g. Yangliuping, Limahe, Zhubu, Jinbaoshan, Baimazhai). The Fe-Ti-V oxide deposits are hosted in gabbroic intrusions, while the sulfide deposits occur in ultramafic-mafic intrusions. Zhou et al. (2008) argued for a genetic relation between the high-

* Tel: +40213060491; fax: +40213181326;
e-mail address: munteanu.marian@igr.ro

Ti Emeishan basalts and the Fe-Ti-V oxide deposits, on the one hand, and between the low-Ti Emeishan basalts and the sulfide deposits, on the other hand.

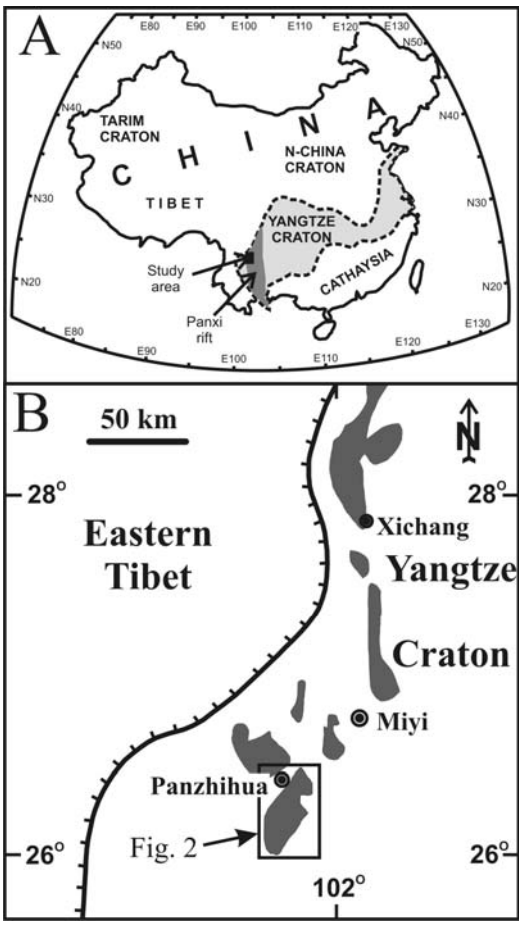

Fig. 1. A. Location of study area in the Panxi rift. B. Tectonic sketch map of the western margin of the Yangtze craton in the south-western part of the Sichuan Province. The Proterozoic intrusions are figured in dark grey.

In this paper we report data resulted from geological observations and geochemical investigations on samples collected during a field trip to several intrusions south of Panzhihua. Based on these data and on the models and hypotheses in the literature, we discuss on the formation of the intrusions and on their Ni-Cu and PGE potential.

2. Geology of the intrusions

The *Datian* intrusive complex is located south-east of the Panzhihua Fe-Ti-V oxide deposit (Fig. 2). It is one of the many batholiths with granitic-dioritic rocks within the late Proterozoic Hannan-Panxi arc (Zhou et al., 2002b); therefore it belongs to the basement of the Panxi rift. Its age is ca. 759 Ma (Li et al., 2003). CGGJC (1986) refer to the Datian complex under the name of Dukou diorite, with an extent of 55 km x 20 km and a petrographic composition dominated by quartz diorite, with variations from hornblende gabbro to granodiorite. Zhao and Zhou (2007a) determined the age of two gabbroic bodies in the north-western margin of the Datian complex to 746 ± 10 Ma and 738 ± 23 Ma. The Datian complex usually displays a gneissic texture and contains enclaves of rocks metamorphosed in the granulite facies (CGGJC, 1986).

Luobodi is a gabbroic intrusion hosting Fe-Ti-V oxide ore. Among the intrusions mineralized with Fe-Ti-V oxides in the Panxi rift, the Luobodi intrusion is located in a western alignment, together with Panzhihua and Malong intrusions (Yao et al., 2001).

Jizicheng is an ultramafic intrusion south of Luobodi. Observations and sampling along a country road that exposes the intrusion almost continuously, showed a spatial zonation, with a marginal zone (ca. 30 m wide) made up of fine-grained peridotite, and a coarser inner zone made up of olivine pyroxenite, the latter showing transitions to more feldspathic compositions (grading to olivine gabbro) in its central part.

Gongshanqing intrusion (ca. 800 m x 500 m) is located at the limit between the dominant Datian quartz diorites (to the east) and the Lixidong granodiorite (to the west). The intrusion is made up of distinct mafic and ultramafic zones. The ultramafic zone is poorly exposed but it was investigated with numerous drill holes and one adit. The exploration conducted during the 1960s indicated Pt+Pd contents up to several g/t and Ni and Cu contents less than 0.5% each.

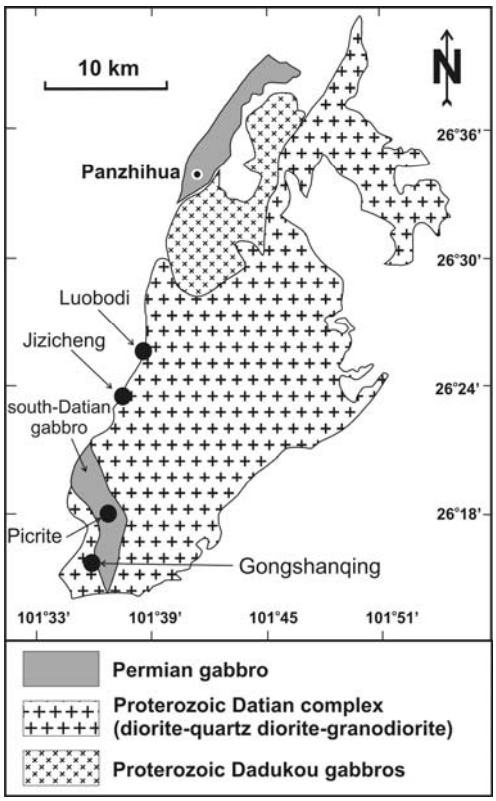

Fig. 2. The Datian intrusive complex and the location of the rocks investigated in this study (geology simplified after Zhao and Zhou, 2007b).

Two *picrite dikes* are figured north-east of the Gongshanqing intrusion on the exploration maps of the Sichuan Bureau for Geology and Mineral Resources. These are limited in their extent (less than 100 m on strike).

The southern part of the Datian Proterozoic complex was intruded by a gabbroic body (Fig. 2) of Permian age (Zhao and Zhou, 2007b, Fig. 2). This intrusion will be referred to hereafter as the *south-Datian gabbros*.

3. Petrography of the Permian intrusions

Luobodi Similar to the rocks in the Panzhihua deposit, the gabbros of the Luobodi intrusion contain olivine. Olivine, pyroxene and plagioclase may be included in Fe-Ti oxides (Fig. 3A,B) but commonly are interstitial to the oxide grains, the latter exhibiting occasional euhedral shapes (Fig. 3C).

Jizicheng The peridotite from the marginal zones is dunitic (~ 90% olivine). The olivine occurs as euhedral crystals (Fig. 3D), commonly less than 1 mm in size (only exceptionally reaching 2 mm), entirely altered to serpentine. A serpentinized mass occurs between the olivine crystals (presumably dominated by former pyroxene oikocrysts). The peridotite gradually passes to pyroxenite, concomitantly increasing its grain size; the olivine crystals become coarser (3-4 mm in size), being accompanied by smaller pyroxene crystals (1-2 mm). Further away from the margins of the intrusion, the proportion of modal olivine gradually decreases to 20-35% in favor of pyroxene, which generates rare porphyric crystals (ca. 6 mm in size). The increasing frequency of the porphyric pyroxene crystals toward the inner parts of the intrusion leads to the generation of equigranular coarser rocks (Fig. 3E). In the coarse equigranular olivine pyroxenite, the pyroxene can be oikocrystic, embaying olivine crystals (Fig. 3F). Plagioclase occurs as interstitial (anhedral to subeuhedral) crystals (Fig. 3G), with increasing proportions in the coarser rocks, where it can exceed 10% modal. Interstitial brown hornblende (Fig. 3H) occurs as a minor phase (2-5%). In the equigranular coarse pyroxenite, olivine may show interstitial position (Fig. 3E). The gabbros occurring in the central part of the intrusion show mesocratic and leucocratic varieties, made up of plagioclase and green hornblende, without pyroxene and olivine.

Gongshanqing Peridotite is the dominant rock type, showing typical cumulate texture (Fig. 4A). The olivine is cumulus, commonly included in pyroxene oikocrysts (Fig. 4B). Brown hornblende and biotite are also oikocrystic, occurring as skeletal crystals interstitial to olivine and pyroxene (Figs. 4A,C). The peridotite shows transitions to pyroxenite. The outcropping mafic rocks are hornblende gabbros (plagioclase and green hornblende), commonly leucocratic to mesocratic.

The picrite dikes show two facies: (a) the fine-grained picrite (Fig. 4D) contains olivine ± pyroxene phenocrysts in a matrix of unoriented plagioclase laths ± anhedral plagioclase crystals, with smaller pyroxene and oxide crystals (magnetite and ilmenite) in the interstices; (b) the medium grained picrite (Fig. 4E) is made up of euhedral olivine phenocrysts ± pyroxene phenocrysts embedded in a groundmass of anhedral plagioclase and euhedral to subeuhedral pyroxene, hornblende, biotite and Fe-Ti oxides. Our samples of *south-Datian gabbros* show simple mineral assemblages, consisting of plagioclase, green hornblende and Fe-Ti oxides. The hornblende may include small plagioclase crystals and Fe-Ti oxide grains (Fig. 4I).

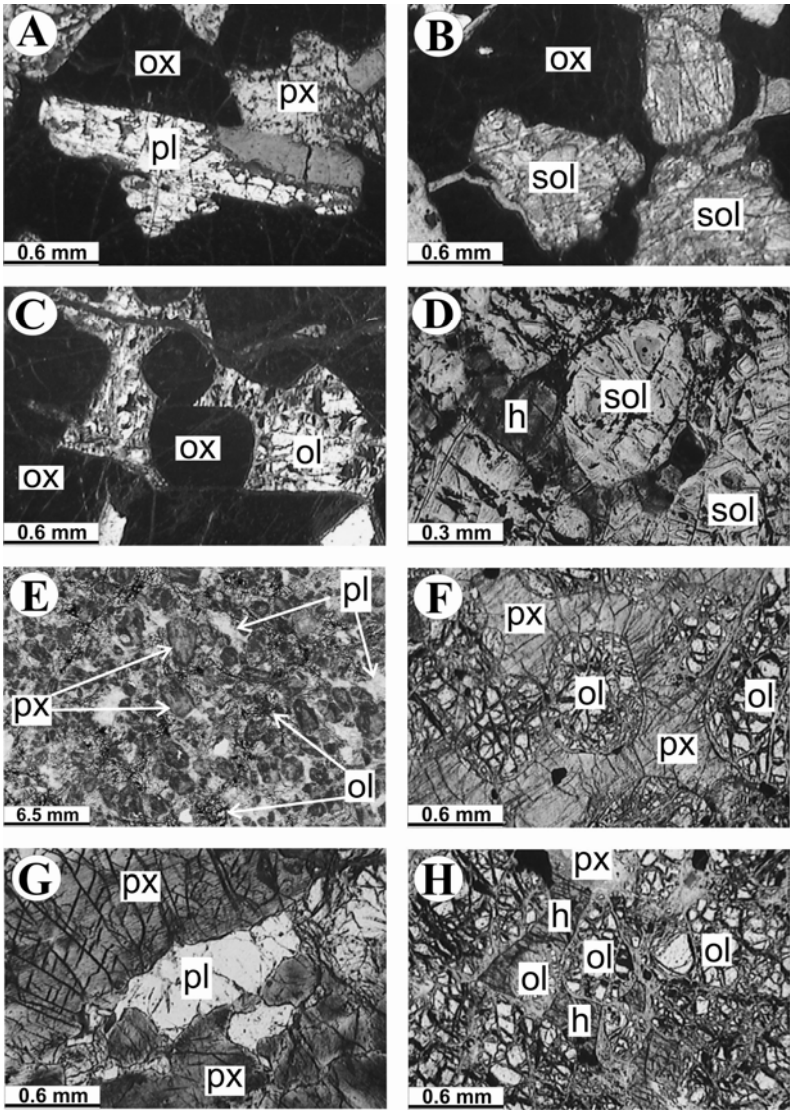

Fig. 3. Mineral relations in the Luobodi (A-C) and Jizicheng (D-H) intrusions. All microscope images (A-E and F-H) were taken in transmitted light, with parallel nicols. Symbols: h= hornblende; ol = olivine; ox = oxide; pl = plagioclase; px = pyroxene; sol = serpentinized olivine. A. Plagioclase crystal included in oxide. B. Serpentinized olivine included in oxide. C. Euhedral oxide grains. D. Dunitic peridotite of the outer zone of the Jizicheng intrusion. Serpentinized olivine crystals and interstitial hornblende. E. Olivine pyroxenite with interstitial anhedral plagioclase. Scanned thin section. F. Pyroxene oikocryst with included olivine crystals. G. Anhedral plagioclase between pyroxene crystals. H. Hornblende oikocrysts with olivine inclusions

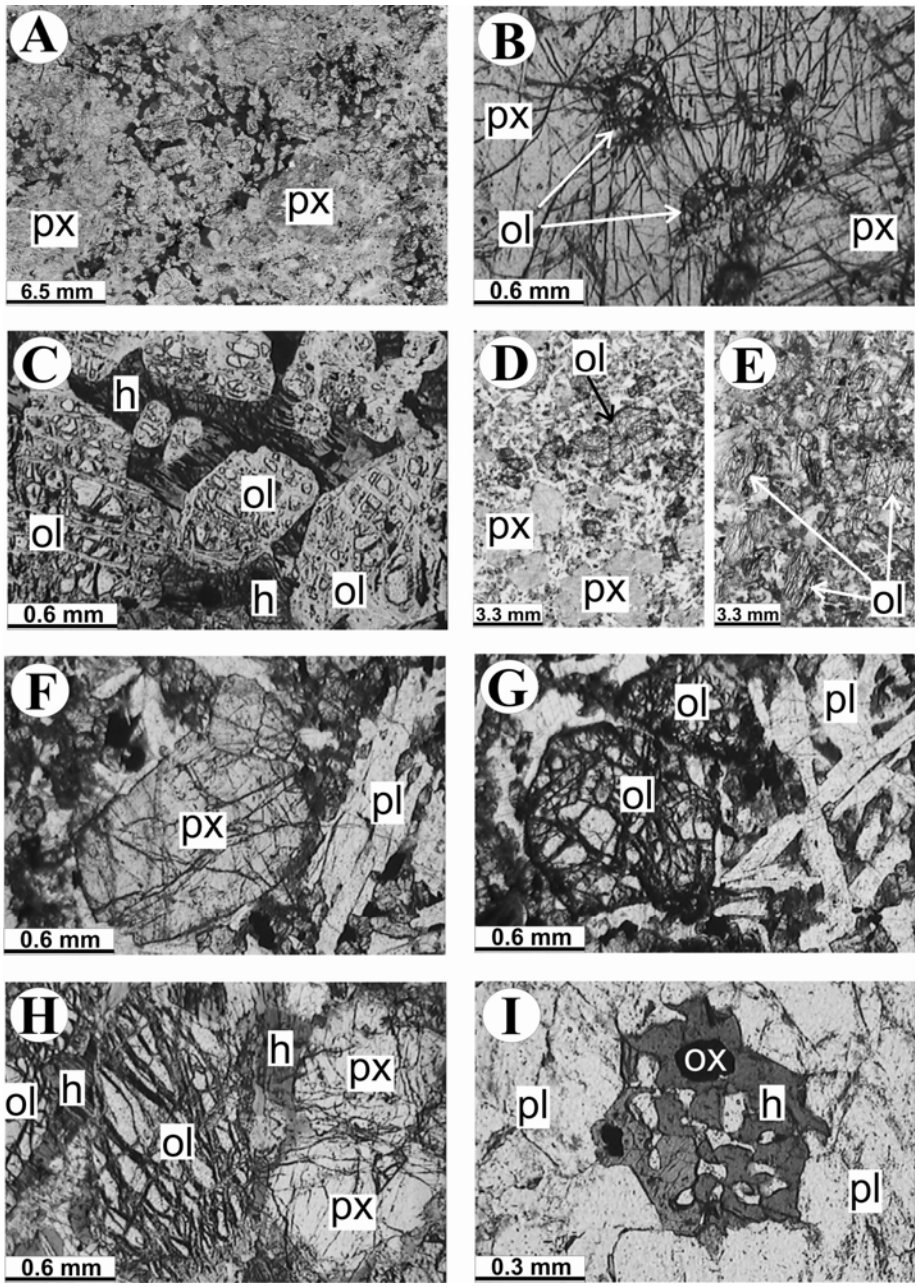

Fig. 4. Mineral relations in the Gongshanqing intrusion (A-C), in the picrite dikes and in the south-Datian gabbros (I). The pictures at the microscope (A-C and F-G) were taken in transmitted light with parallel nicols. Symbols: h= hornblende; ol = olivine; ox = oxide; pl = plagioclase; px = pyroxene. A. Peridotite with hornblende oikocrysts (dark) between pyroxene oikocrysts (px), both including olivine crystals. B. Olivine crystals in pyroxene oikocryst. C. Olivine crystals in hornblende oikocryst. D. Fine-grained facies of picrite, with porphyric olivine and pyroxene in a matrix made up of euhedral plagioclase laths and interstitial pyroxene. Scanned thin section. E. Medium-grained facies of picrite, with olivine crystals in a matrix made up of anhedral plagioclase, pyroxene and hornblende. Scanned thin section. F. Fine-grained facies. Euhedral plagioclase, porphyric pyroxene, surrounded by small euhedral pyroxene, oxide, euhedral to subeuhedral plagioclase, anhedral hornblende. G. Fine-grained facies. Euhedral plagioclase, porphyric olivine and interstitial pyroxene, oxide and hornblende. H. Medium-grained facies. Porphyric pyroxene and olivine with interstitial hornblende and plagioclase. I. South-Datian gabbro. Hornblende with inclusions of plagioclase and oxide.

Table 1. Major and trace element contents of the investigated intrusive rocks. Dt = Datian; gbb = gabbro; Gg = Gongshanqing; Jzc = Jizicheng; Lbd = Luobodi; mgt = Fe-Ti-V oxide ore; per = peridotite; pxt = pyroxenite; qd = quartz diorite; sDg = south-Datian gabbro; bdl = below detection limit.

Sample	Dt1	Dt5	Dt7	Dt7A	Dt8	Dt9	Dt10	Dt11	Dt12
Latitude	26.35968	26.26312	26.26312	26.26438	26.26467	26.26439	26.26378	26.42225	26.42225
Longitude	101.7639	101.6053	101.6053	101.6076	101.6071	101.6071	101.6062	101.6348	101.6348
Lithology	qd	per	gbb	per	per	per	per	pxt	pxt
Intrusion	Dt	Gg	Gg	Gg	Gg	Gg	Gg	Lbd	Lbd
SiO_2 %	64.78	41.08	56.95	45.19	47.21	40.64	40.38	18.73	19.94
TiO_2	0.44	0.81	0.54	2.19	0.9	0.76	0.78	11.45	10.46
Al_2O_3	17.02	4.32	18.47	7.59	3.94	3.46	3.63	8.51	9.23
Fe_2O_3	4.17	15.32	5.52	14.7	13.11	15.37	15.25	49.13	47.76
MnO	0.05	0.18	0.1	0.18	0.19	0.18	0.18	0.27	0.27
MgO	2.32	26.85	3.82	19.53	22.38	29.42	28.48	5.76	6.7
CaO	4.17	3.82	5.18	5.91	8.76	2.89	3.1	3.26	2.28
Na_2O	3.93	0.51	5.32	1.11	0.51	0.41	0.36	0.53	0.38
K_2O	2.32	0.31	1.54	0.24	0.2	0.22	0.23	0.09	0.09
P_2O_5	0.13	0.07	0.16	0.16	0.07	0.08	0.09	0.06	0.03
LOI	0.6	5.8	2.3	2.6	1.9	5.5	6.5	2.1	2.6
S	bdl	0.11	bdl	bdl	0.14	bdl	bdl	0.38	0.33
Total	99.94	99.18	99.92	99.44	99.31	98.99	99.05	100.27	100.07
Sc ppm	7	14	11	22	33	11	13	27	28
V	74	133	104	219	167	113	122	1643	1587
Cr	37	357	28	381	253	292	372	0.5	bdl
Co	11	96	11	62	57	107	102	121	137
Ni	21	1297	31	1029	994	1579	1503	29	33
Cu	3	57	10.5	288	245	44	53	69	63
Ga	19	7.2	19	12.2	7.1	5.6	6.7	28.2	28
Rb	92	7.3	42.2	2.4	5.1	5.1	5.7	2.1	2.1
Sr	476	140	672	240	102	120	106	202	170
Y	5	8.4	11	18.2	10.7	6.5	8	8.1	7.2
Zr	77	49	106	124	47	44	48	34	32
Nb	6.2	6.4	4.5	12.6	4.2	4.7	5.6	6.1	5.7
Ba	494	67	369	78	40	43	48	216	388
Cs	4.1	0.4	0.5	0.8	0.4	0.2	0.3	0.2	0.3
La	10.2	6.1	15.9	12.5	4.9	4.8	5.5	3.1	2.6
Ce	20.3	15.2	34.9	33.2	13	11.8	13.6	8.6	6.9
Pr	2.3	2.0	4.2	4.5	1.8	1.6	1.8	1.4	1.1
Nd	8.6	8.8	17.6	21.5	9.1	7.2	8.5	7.4	6.4
Sm	1.56	1.92	2.83	4.41	2.11	1.58	1.76	1.71	1.49
Eu	0.62	0.62	0.82	1.4	0.72	0.51	0.56	0.91	0.96
Gd	1.28	1.79	2.26	4.1	2.17	1.49	1.69	1.9	1.67
Tb	0.22	0.33	0.39	0.72	0.41	0.26	0.31	0.34	0.29
Dy	0.85	1.51	1.74	3.34	1.97	1.26	1.37	1.56	1.37
Ho	0.15	0.27	0.33	0.61	0.36	0.22	0.25	0.27	0.24
Er	0.38	0.71	0.88	1.53	0.89	0.58	0.64	0.67	0.59
Tm	0.06	0.11	0.15	0.24	0.14	0.09	0.1	0.09	0.08
Yb	0.36	0.64	0.94	1.36	0.77	0.51	0.58	0.53	0.49
Lu	0.05	0.1	0.14	0.2	0.12	0.08	0.08	0.08	0.07

Hf	2.2	1.4	3	3.7	1.5	1.4	1.3	1.2	1.3
Ta	0.3	0.4	0.2	0.7	0.2	0.2	0.3	0.3	0.3
Pb	1.08	0.88	5.69	1.04	0.79	0.78	0.9	0.6	0.73
Th	2.5	0.9	2.7	1.8	0.7	0.8	0.7	0.1	0.2
U	0.6	0.2	0.7	0.4	0.2	0.2	0.2	bdl	bdl
Pd ppb	bdl	bdl	bdl	28	36	15	19	bdl	bdl
Pt	bdl	bdl	bdl	19	28	15	19	bdl	bdl
Ti/Y	528	579	295	722	505	702	585	8481	8717
Zr/Nb	15.5	5.8	9.7	6.8	4.4	6.8	6.0	4.2	4.5
La/Yb	28.3	9.5	16.9	9.2	6.4	9.4	9.5	5.8	5.3
Cu/Pd	0	0	0	10298	6794	2957	2769	0	0
Cu/Zr	0.04	1.17	0.10	2.32	5.22	1.00	1.11	2.01	1.94

Table 1 (continued)

Sample	Dt13	Dt15	Dt16	Dt17	Dt18	Dt19	Dt20	Dt22	Dt25
Latitude	26.42225	26.38146	26.38153	26.38135	26.38158	26.38195	26.38195	26.38257	26.38657
Longitude	101.6348	101.6145	101.6148	101.6142	101.6138	101.613	101.613	101.6129	101.6132
Lithology	mgt	pxt	pxt	pxt	pxt	pxt	gbb	pxt	pxt
Intrusion	Lbd	Jzc	Jzc	Jzc	Jzc	Jzc	Jzc	Jzc	Jzc
SiO_2 %	4.91	38.97	38.94	45.13	43.59	48.36	46.47	44.15	45.68
TiO_2	15.82	0.28	0.31	0.71	0.75	0.82	0.62	0.61	0.84
Al_2O_3	4.3	1.48	1.74	3.18	3.53	3.37	11.85	2.32	5.83
Fe_2O_3	71.03	12.48	13.35	13.6	15.52	12.03	11.51	14.27	12.36
MnO	0.36	0.14	0.15	0.19	0.21	0.19	0.15	0.19	0.18
MgO	2.84	33.1	32.05	22.58	22.49	19.4	15.65	24.69	18.9
CaO	0.17	0.04	0.07	11.96	10.77	14.88	11.49	10.21	12.99
Na_2O	0.01	bdl	bdl	0.3	0.33	0.41	1.5	0.25	0.58
K_2O	bdl	bdl	bdl	bdl	bdl	bdl	0.11	bdl	0.06
P_2O_5	0.05	0.01	0.02	0.01	0.01	bdl	0.02	bdl	0.02
LOI	0.3	12.4	12.4	1.7	2.2	0.1	0.4	2.7	2.1
S	bdl	bdl	bdl	bdl	bdl	bdl	bdl	bdl	bdl
Total	99.82	98.92	99.04	99.37	99.41	99.58	99.78	99.40	99.56
Sc ppm	18	7	8	42	39	57	31	36	43
V	1760	63	61	167	185	241	156	145	184
Cr	37	314	255	223	321	126	347	201	257
Co	11	113	106	78	91	49	64	97	65
Ni	54	2268	1914	934	1071	480	445	1082	699
Cu	31	14	74	56	37	101	10	14	23
Ga	28.1	3.3	3.3	5.2	5.8	5.9	11.7	4.4	8
Rb	0.5	bdl	bdl	0.5	0.6	0.5	1.2	bdl	1.3
Sr	576	3.3	6.6	76	101	104	526	57	210
Y	3.7	3	2.4	9.1	8.1	12.1	7.2	8.5	10.6
Zr	28	11.1	8.3	18.1	15.7	21.9	14.8	15.8	22.8
Nb	5.6	0.6	0.6	0.4	0.3	0.5	0.4	0.2	0.6
Ba	253	bdl	bdl	bdl	5	bdl	45	bdl	18
Cs	0.1	0.1	0.1	bdl	0.1	bdl	0.2	bdl	0.2
La	2.2	0.9	0.8	1.5	1.3	1.7	1.8	1.2	2
Ce	5.5	2.7	2.4	5.4	4.7	6.8	5.3	4.4	6.8
Pr	0.8	0.44	0.38	1.03	0.91	1.34	0.93	0.89	1.25
Nd	3.8	2.4	2	5.7	5.2	8.1	5.4	5.7	7.7

Sm	0.87	0.62	0.48	1.68	1.56	2.33	1.43	1.56	2.07
Eu	0.36	0.2	0.2	0.59	0.55	0.79	0.66	0.54	0.72
Gd	0.89	0.69	0.54	1.92	1.81	2.59	1.65	1.84	2.2
Tb	0.15	0.12	0.09	0.36	0.34	0.49	0.29	0.32	0.41
Dy	0.67	0.52	0.47	1.77	1.59	2.29	1.41	1.6	1.89
Ho	0.12	0.1	0.08	0.3	0.28	0.41	0.26	0.29	0.36
Er	0.3	0.25	0.23	0.75	0.7	1.03	0.6	0.7	0.84
Tm	0.04	0.04	0.03	0.1	0.1	0.15	0.09	0.09	0.13
Yb	0.24	0.23	0.19	0.59	0.58	0.87	0.51	0.58	0.76
Lu	0.04	0.04	0.03	0.09	0.08	0.12	0.07	0.08	0.1
Hf	1	0.4	0.3	0.8	0.8	1.1	0.8	0.7	1.1
Ta	0.3	bdl	bdl	bdl	bdl	bdl	bdl	bdl	bdl
Pb	0.08	3.62	0.53	0.05	0.02	0.11	0.06	0.02	0.2
Th	bdl	bdl	bdl	bdl	bdl	bdl	bdl	bdl	bdl
U	bdl	bdl	bdl	bdl	bdl	bdl	bdl	bdl	bdl
Pd ppb	bdl	17	22	15	bdl	17	bdl	bdl	bdl
Pt	bdl	32	17	13	9	17	6	3	2
Ti/Y	25654	560	775	468	556	407	517	431	475
Zr/Nb	7.6	3.7	3.5	2.0	1.9	1.8	2.1	1.9	2.2
La/Yb	9.2	3.9	4.2	2.5	2.2	2.0	3.5	2.1	2.6
Cu/Pd	0	795	3361	3743	0	5963	0	0	0
Cu/Zr	1.12	1.22	8.91	3.10	2.36	4.63	0.71	0.87	1.02

Table 1 (continued)

Sample	Dt27	Dt28	Dt29	Dt30	Dt31	Dt32	Dt33	Dt34	Dt35	Dt36
Latitude	26.38655	26.38654	26.28963	26.28971	26.28958	26.28844	26.28803	26.29106	26.29106	26.29008
Longitude	101.6129	101.6112	101.6369	101.6372	101.6373	101.6391	101.6047	101.622	101.622	101.6129
Lithology	pxt	per	qd	gbb	gbb	gbb	granite	picrite	picrite	picrite
Intrusion	Jzc	Jzc	Dt	sDg	sDg	sDg	Dt	dike 1	dike 1	dike 2
SiO_2 %	38.54	39.78	59.08	45.04	45.31	45.19	64.39	46.78	43.49	46.57
TiO_2	0.32	0.36	0.56	2.97	3.27	3.45	0.43	1.52	1.12	2.65
Al_2O_3	2.04	3.44	18.14	13.94	13.94	14.21	15.67	10.36	6.06	9.2
Fe_2O_3	18.14	14.67	5.69	17.72	17.58	16.59	4.75	12.19	12.48	12.46
MnO	0.21	0.18	0.08	0.17	0.17	0.18	0.1	0.17	0.16	0.16
MgO	30.5	31.01	3.47	5.85	5.82	5.68	2.86	13.61	25.81	14.53
CaO	2.57	3.09	6.65	9.23	8.29	9.19	2.48	9.97	5.29	7.73
Na_2O	0.07	0.17	4.13	2.44	2.72	2.6	4.53	1.79	1.09	1.59
K_2O	bdl	0.05	1.14	0.9	1.09	0.89	2.98	0.56	0.47	1.48
P_2O_5	0.02	0.04	0.17	0.17	0.16	0.16	0.12	0.15	0.12	0.31
LOI	6.8	6.2	0.8	1.5	1.6	1.8	1.6	2.6	3.3	2.9
S	bdl	bdl	bdl	0.35	0.29	0.25	bdl	0.1	0.11	0.17
Total	99.22	99.03	99.92	100.28	100.24	100.19	99.91	99.80	99.50	99.75
Sc ppm	13	10	12	29	29	29	12	33	17	24
V	94	88	112	628	579	503	85	278	169	245

Cr	91	141	34	1.4	0.8	1.5	38	116	290	206
Co	117	109	11.0	40	36	31	10	42	80	48
Ni	1940	1659	30	34	11	6	31	386	1548	641
Cu	29.6	45.8	1.5	79	52	44	5.1	94	72	103
Ga	3.5	4.6	18.6	22.6	20.7	21.6	16.6	14.2	8.8	15.2
Rb	0.5	1.1	27.9	21.8	32.1	20.1	83	13.6	11.2	31.5
Sr	24	114	678	394	412	414	455	338	244	618
Y	2.2	3.2	11.5	24	22.3	25.3	21.1	18.8	12.3	23.5
Zr	6.4	15.1	95	111	106	117	114	109	81	244
Nb	0.2	1.1	4.2	18.5	18.8	22.2	7.2	12.3	11.3	35.2
Ba	6	21	365	207	264	219	627	182	147	630
Cs	0.1	0.1	1	0.5	0.5	0.3	2.3	1.1	0.3	2.7
La	0.7	1.5	16.2	17.2	16.4	18.2	16	13.9	12.6	42.5
Ce	1.7	3.8	37	40	38	42	37	34	29	96
Pr	0.29	0.57	4.38	5.14	4.86	5.41	4.84	4.44	3.71	11.89
Nd	1.6	2.7	17.9	22.8	21.8	24.4	21.3	20.4	16.4	50.3
Sm	0.41	0.63	3	4.53	4.25	4.81	4.56	3.95	2.98	7.78
Eu	0.16	0.26	0.94	1.53	1.42	1.58	0.92	1.29	0.93	2.2
Gd	0.54	0.68	2.5	4.59	4.19	4.76	4.18	3.76	2.67	5.91
Tb	0.09	0.12	0.42	0.87	0.81	0.89	0.77	0.69	0.47	1
Dy	0.44	0.54	1.93	4.04	3.89	4.36	3.5	3.2	2.15	4.36
Ho	0.08	0.1	0.36	0.79	0.72	0.81	0.67	0.62	0.4	0.76
Er	0.21	0.29	1	2.09	1.89	2.12	1.76	1.62	1	1.89
Tm	0.03	0.04	0.16	0.32	0.29	0.35	0.27	0.25	0.16	0.28
Yb	0.18	0.29	0.99	1.96	1.81	2.03	1.64	1.53	0.91	1.66
Lu	0.03	0.04	0.16	0.28	0.26	0.29	0.24	0.21	0.13	0.23
Hf	0.3	0.4	2.9	3.3	3.3	3.8	3.7	3.3	2.5	7.2
Ta	bdl	bdl	0.2	0.9	1	1.2	0.3	0.7	0.7	1.8
Pb	5.41	1.22	1.63	2.37	3.02	2.02	8.23	1.54	1.56	2.75
Th	bdl	0.1	4.4	3	2.9	3	4.8	2	1.6	5.4
U	bdl	bdl	0.9	0.6	0.5	0.6	0.5	0.4	0.4	1.2
Pd ppb	bdl	14	bdl	bdl	bdl	bdl	bdl	10	bdl	bdl
Pt	15	8	bdl	bdl	bdl	bdl	bdl	9	5	5
Ti/Y	873	675	292	743	880	818	122	485	546	677
Zr/Nb	2.9	4.7	8.2	4.6	4.8	4.6	5.4	5.8	6.6	10.4
La/Yb	3.9	5.2	16.4	8.8	9.1	9.0	9.8	9.1	13.8	25.6
Cu/Pd	0	3271	0	0	0	0	0	9362	0	0
Cu/Zr	4.63	3.03	0.02	0.71	0.49	0.38	0.04	0.86	0.89	0.42

4. Samples and analytical methods

The coordinates of each sample are given in Table 1. Three samples come from the Datian intrusive complex. Three further samples were collected from the south-Datian gabbros. Three samples were taken from a former exploration site in the Luobodi intrusion. All of them are mineralized with Fe-Ti-V oxides (massive to semi-massive ore). Six samples (one gabbro and five ultramafic rocks) come from the Gongshanqing intrusion (from outcrops, adit and drill cores spread around drill sites). Other three samples were taken from picrite blocks occurring on two creeks downstream from the picrite dikes (one from the fine-grained variety and two from the medium-grained type). We also analyzed ten samples from the Jizicheng intrusion (four from the marginal dunite, five from the inner olivine pyroxenite and one gabbro from the central part of the intrusion).

Bulk rock analyses were performed at the ACME laboratories in Vancouver. The samples were mixed with lithium metaborate/tetraborate and fused in a furnace. The cooled beads were dissolved in ACS grade nitric acid. Loss on ignition was determined by weight difference after ignition at 1000°C. The major elements and Ba were analyzed by ICP-OES (inductively coupled plasma optical emission spectrometry) using a Varian spectrometer. Sulfur was analyzed by combustion, using a LECO CS-200 analyzer. Trace elements were analyzed by ICP-MS (inductively coupled plasma-mass spectrometry), using a Perkin-Elmer instrument, after lithium metaborate fusion and dilute nitric acid digestion (Cs, Hf, Nb, Rb, Sr, Ta, Th, U, V, Zr, Y and REE) or after Aqua Regia digestion (Cu, Pb, Ni, Co, Cr, Pd and Pt). The accuracy and precision of the trace element data were about 5%.

5. Results

The mineralogical and chemical composition of the investigated samples reflect the diversity of the investigated material (Table 1). In order to characterize the analyzed samples, we used spider diagrams of REE (normalized to chondrite) and of the incompatible elements Cs, Rb, Ba, Th, U, Nb, Ta, K, La, Ce, Pb, Pr, Sr, P, Nd, Zr, Sm, Eu, Ti, Dy, Y, Yb, Lu (normalized to the primitive mantle). The normalizing values for chondrite and primitive mantle were taken from Sun and McDonough (1989). The spider diagrams of the samples from each investigated intrusion are given in Figs. 5 and 6.

Datian. The large ion lithophile elements (K, Rb, Cs, Sr, Ba) are enriched relative to the high field strength elements (Zr, Nb, Hf, Ta), a feature consistent with the formation of the complex by arc magmatism. The Lixidong granite shows incompatible elements patterns similar to those of the quartz diorite. The REE show sloped patterns, with remarkable differentiation between LREE and HREE (La_N/Lu_N = 7-22).

Gongshanqing. In general, REE patterns of peridotites show flat patterns of LREE and HREE (La_N/Sm_N = 1.1-1.8, Er_N/Lu_N = 1-1.2) relative to MREE (Sm_N/Ho_N = 2.2-2.7). A saprolitic peridotite from the adit shows similar trend but increased REE contents. A steeper descending pattern is shown by the gabbro (La_N/Lu_N = 12). The peridotites display small variations of the normalized values of the incompatible elements. The saprolitic peridotite shows negative anomalies of Rb, K and P. The gabbro exhibits high values of LILE and negative anomalies for HSFE, similar to arc-related/crustal magmas.

Jizicheng. The intrusion has lower contents of incompatible elements, compared with Gongshanqing. REE are lower in the peridotites from the marginal zone of the intrusion than in the pyroxenites of the inner part, all showing flat trends (La_N/Lu_N = 1.5-3). The peridotites show steeper slope between the MREE and HREE (Tb_N/Ho_N = 1.7-1.8). Pyroxenites show depletion of LREE and HREE relative to MREE. The gabbros have trends similar with those of pyroxenites, showing no Eu anomaly. This suggests the formation of the gabbro by the local increase of the proportion of interstitial melt, without plagioclase fractionation/accumulation,

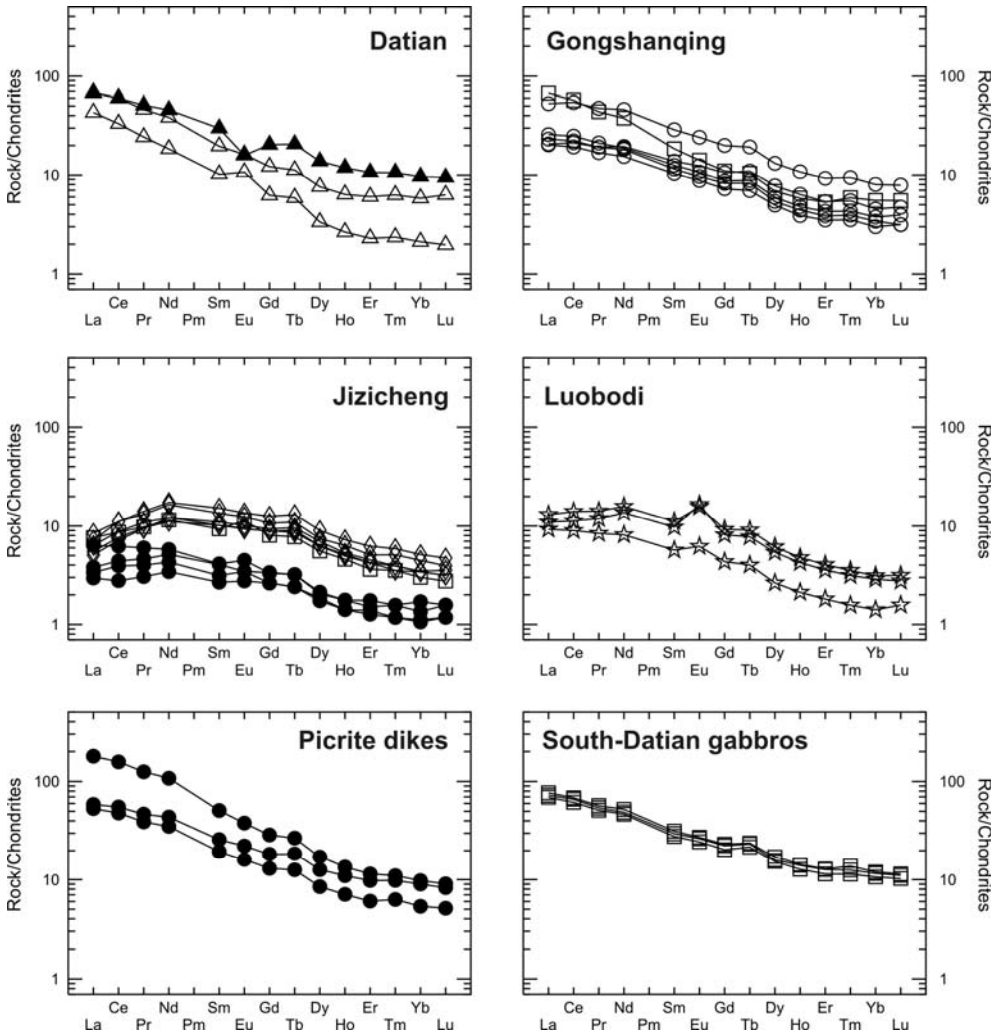

Fig. 5. Chondrite-normalized REE patterns for the investigated intrusions. Chondrite normalization values from Sun and McDonough (1989).

in agreement with the petrographic observations, which indicate plagioclase as an intercumulus phase.

Luobodi. The three ore samples exhibit similar trends of incompatible elements, with marked positive anomalies for Cs, Ba, Sr and Ti, and negative anomalies for Rb, Th and U. The REE patterns exhibit positive Eu anomalies. All samples have high metal contents (33-50% Fe, 6-9.5% Ti, 0.16-0.17% V).

Picrite dikes show descending REE patterns (La_N/Lu_N = 7-20) and relatively uniform trends of incompatible elements, only with small negative anomalies for Rb and P.

The three samples of **south-Datian gabbros** show remarcably homogeneous compositions, with incompatible elements and REE patterns similar to those of the picrite dikes, only flatter (La_N/Lu_N = 6.6-6.8), suggesting less differentiation of the parental magma.

6. Discussions

Except for the Datian complex, which is Proterozoic, the investigated intrusions are Permian, related to the mantle plume magmatism the other rocks in the intrusion of the Emeishan large igneous province.

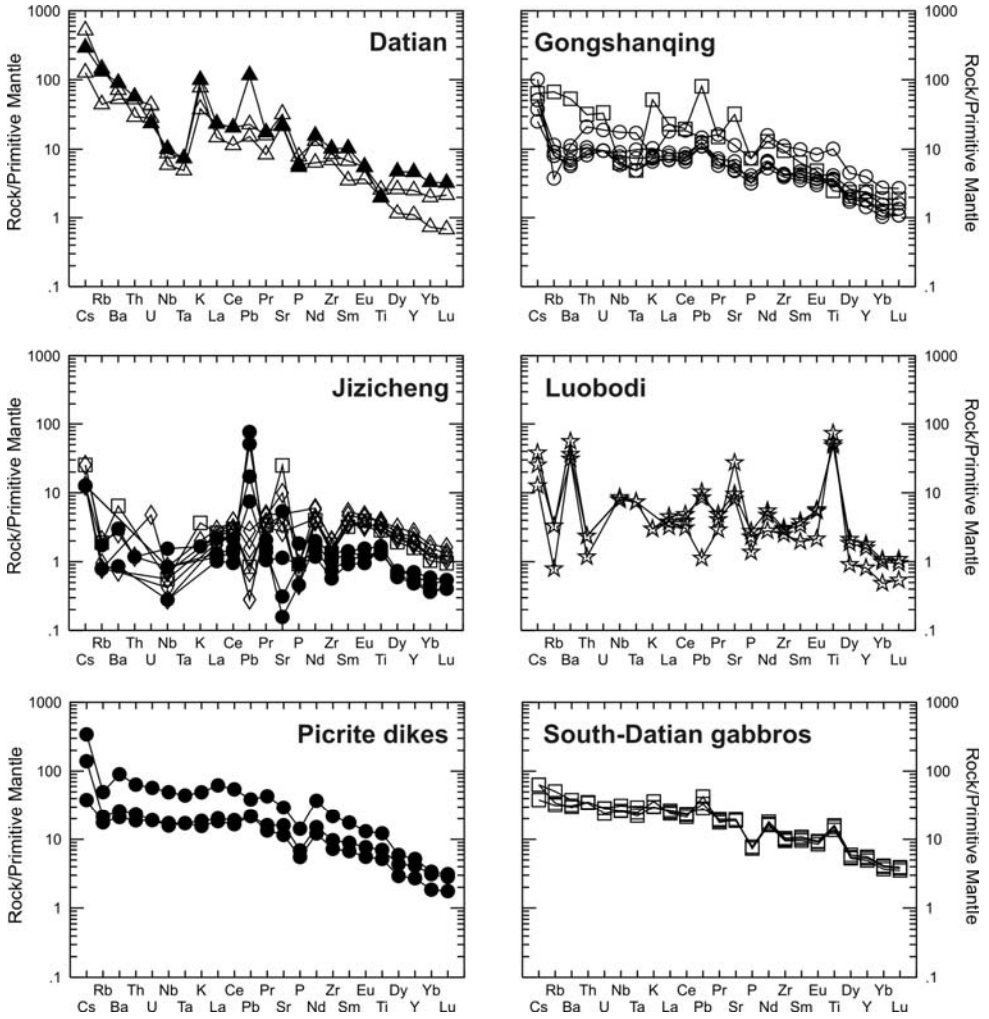

Fig. 6. Primitive mantle-normalized patterns of the incompatible elements in the investigated intrusions. Primitive mantle normalization values from Sun and McDonough (1989).

The anorogenic geotectonic setting is supported by the composition of picrite dikes and south-Datian gabbros, which have contents of incompatible elements close to ocean island basalts, as illustrated in Fig. 7. The relative depletion of LREE in the olivine pyroxenite from Jizicheng (Fig. 5) reflects clinopyroxene accumulation, whereas LREE have smaller partition coefficients in clinopyroxene than those of the other REE (e.g. McKay, 1989; Hack et al., 1994). The patterns of the incompatible elements in the ore from Luobodi (Fig. 6) is similar to the trends of the gabbros in the Panzhihua (Zhou et al., 2005) and Baima (Shellnutt et al., 2009) Fe-Ti-V deposits. The ore in the Luobodi intrusion displays visible positive Eu anomaly (Fig. 5), suggesting the entrapment of cumulus plagioclase in the oxide ore. One problem recently raised for the intrusions and ore deposits in the Panxi rift is the correspondence (genetic affinity) between different types of rocks/deposits and the two geochemical types of Emeishan basalts (Zhou et al., 2008). Among the studied rocks, only the picrite dikes and south-Datian gabbros show distributions of incompatible elements that suggest the lack of substantial fractionation

processes. The Ti/Y ratio is higher than 500 in most analyzed samples, irrespective of rock types, which would classify all intrusions in the high-Ti geochemical type. Xiao et al. (2004, Fig. 4) show that high-Ti basalts have La/Yb>10 and Zr/Nb<10, while low-Ti basalts show La/Yb<10 and Zr/Nb ratios that overlap the variation field of high-Ti basalts. An examination of our results shows that most samples (including gabbros, oxide ore and ultramafic cumulates) have La/Yb<10, similar to low-Ti basalts of Xiao et al. (2004). The Zr/Nb ratio is typical for low-Ti basalts (>10) only in the Jizicheng intrusion, where it can be correlated with the Ti/Y ratio lower than 500 in the samples from the inner zone made up of olivine pyroxenite.

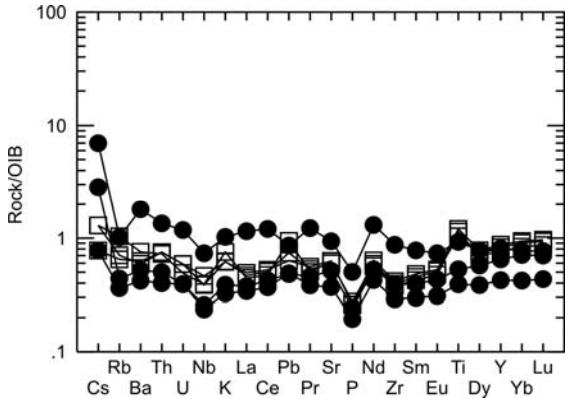

Fig. 7. Spider diagram of the incompatible elements in the picrite dikes (solid circles) and south-Datian gabbros (open squares) normalized to ocean island basalts. Normalization values from Sun and McDonough (1989).

The presence of economic Ni-Cu and PGE mineralization in several mafic-ultramafic intrusions from the Panxi rift is a main reason for the investigation of the economic potential of other intrusions. The genesis of mafic-ultramafic intrusions involves partial melt of the mantle, the ascent of the resulted magmas and their emplacement in the crust. Because of their high affinity for sulfides, the PGE are readily removed from the magma even at low ratios of sulfide exsolution and fractionation. Hence, one critical condition for the occurrence of mineable PGE mineralization is the absence of any pre-emplacement sulfide fractionation from the parental magma. The PGE contents in most ultramafic rocks at Gongshanqing and Jizicheng (22-64 ppb) are similar to or higher than those of the PGE-undepleted mafic magmas (Greenough and Owen 1992; Barnes and Picard 1993; Brügmann et al. 1993). Considering the cumulate nature of these rocks and the fact that both Pt and Pd behave incompatible in olivine and pyroxene, it is reasonable to consider that the PGE contents in these rocks indicate the presence of sparsely disseminated PGE-rich sulfide grains. This is consistent with the higher sulfur content in the PGE-rich samples (Table 1).

The Cu/Zr ratio can be used as an indicator of sulfide fractionation before magma emplacement. Both Cu and Zr are strongly incompatible in most silicate phases, but Cu concentrates in sulfides. It is considered that magmas which did not experience sulfide fractionation have Cu/Zr ratios close to 1 (Lightfoot et al., 1994; Li and Naldrett, 1999; Wang et al., 2006), while in the case of a pre-emplacement sulfide fractionation, Cu/Zr ratio would be less than 1, because a significant part of the Cu fractionated with the sulfides. The ultramafic rocks from Gongshanqing (Table 1) display Cu/Zr ratios both close to 1 or higher (2.3-5.2). This suggests the absence of any pre-emplacement sulfide fractionation and the occurrence of zones with sulfide accumulation, which induced the increase of Cu content. A similar situation occurs at Jizicheng, which contains rocks formed from magmas that did not experience sulfide fractionation or sulfide accumulation (Cu/Zr ratios close to 1) and rocks containing accumulated sulfides (Cu/Zr in the range 2.4-8.9). The gabbro from Gongshanqing, with Cu/Zr = 0.1, would suggest sulfide fractionation, in contrast with the other rocks in the intrusion. This feature might indicate a substantial contribution of crustal material to the genesis of the gabbros of the Gongshanqing intrusion. A similar spatial association between ultramafic cumulates and crustal melts was inferred for the Lengshuiqing Ni-Cu deposit in the Proterozoic basement of the Panxi rift (Munteanu et al., 2010). In the case of the south-Datian gabbros, with Cu/Zr ratio be-

tween 0.4 and 0.7, sulfide fractionation probably occurred in the parental magma at greater depth. The picrite dike that shows Cu/Zr ratios slightly lower than 1, probably formed from magmas that did not reach sulfide saturation. The picrite dike having Cu/Zr = 0.4 contains excess Zr compared with the other dike, a feature that probably resulted from assimilation of crustal material. This is consistent with the higher contents of K, P and Rb.

The Cu/Pd ratio in a magma is sensitive to sulfide fractionation since the Pd partition coefficient in sulfide is much higher than Cu partition coefficient. Therefore, in the case of sulfide fractionation, Pd is removed from the magma at much higher rate than Cu, inducing the increase of Cu/Pd above the original ratio, which is supposed to be within the mantle range (Barnes et al., 1993; Barnes et al., 2004; Barnes and Lightfoot, 2005). In this respect, the Cu/Pd ratios of the ultramafic samples in our set (Table 1), with values within the mantle range (1,000-10,000) suggest a parental magma that did not experience sulfide fractionation before the formation of the actual intrusions.

The Gongshanqing and Jizicheng intrusions, dominated by ultramafic cumulates were probably generated in wider zones of magmatic conduits. Similar genesis was inferred for several ultramafic-mafic intrusions in the Panxi rift, such as Zhubu (Zhu et al., 2007), Limahe (Tao et al., 2007a), Jinbaoshan (Wang et al., 2005; Tao et al., 2007b) and Baimazhai (Wang and Zhou, 2006), based on their composition different than the normal compositions of the mafic magmas. In the petrogenetic and metallogenetic models involving magma conduits, mafic crystals ± immiscible sulfide droplets are transported from a staging chamber to shallower levels in the crust. When the section of a conduit increases, the flow of magma is slowed down and cannot carry the denser mafic crystals ± sulfide melt, which accumulate, generating ultramafic rocks ± Ni-Cu or PGE mineralization. Although the association with magma conduits seems to be characteristic for Ni-Cu deposits (Li et al., 2001; Maier et al., 2001), it facilitates the contact of the immiscible sulfides with large quantities of flowing magma, contributing to their enrichment in PGE. Such a process was invoked to explain the genesis of the Jinbaoshan PGE deposit (Wang et al., 2005; Tao et al., 2007b) and could be applied in the case of the Gongshanqing and Jizicheng intrusions, as well.

7. Conclusions

This work produced and interpreted data on several intrusions of the two main petrographic-metallogenetic associations related to the Emeishan large igneous province: gabbroic intrusions with Fe-Ti-V oxides and ultramafic-mafic intrusions with Ni-Cu(-PGE) sulfide mineralization. The geochemical investigation could not evidence a correlation between the studied intrusions and the high-Ti and low-Ti Emeishan basalts. The Cu/Pd and Cu/Zr ratios of the ultramafic rocks investigated here suggest the genesis from Cu- and PGE-fertile magmas. The Cu/Pd and Cu/Zr ratios are similar in the Gongshanqing and Jizicheng intrusions, suggesting that the Jizicheng intrusion could contain a PGE-rich mineralization like the one discovered in the Gongshanqing intrusion.

Acknowledgements

This research was financially supported by Anglo Platinum Ltd. The work was logistically arranged by Sichuan Anglo Platinum Exploration Ltd and Sichuan Bureau of Geology and Mineral Resources. The field work was assisted by Geological Team 106 and San Zhou Mining Company. The manuscript benefited from the remarks made by Haino Uwe Kasper (University of Cologne) and by an anonymous reviewer.

References

Ali, J.R., Thompson, G.M., Zhou, M.-F., Song, X., 2005. Emeishan large igneous province, SW China. Lithos, 79, 475–489.

Barnes, S.-J. & Lightfoot, P.C., 2005. Formation of magmatic nickel-sulfide ore deposits and

processses affecting their copper and platinum-group element contents. In Econ. Geol. 100th Anniversary Volume (Hedenquist, J.W., Thompson, J.F.H., Goldfarb, R.J. & Richards, J.P., eds.), 179-213.

Barnes, S.-J., Picard, C.P., 1993. The behaviour of platinum-group elements during partial melting, crystal fractionation and sulfide segregation: an example from the Cape Smith fold belt, northern Quebec. Geochim Cosmochim Acta, 57, 79–87.

Barnes, S.-J., Couture, J.-F., Sawyer, E.W., Bouchaib, C., 1993. Nickel-copper occurrences in the Belleterre-Angliers Belt of the Pontiac subprovince and the use of Cu-Pd ratios in interpreting platinum-group element distributions. Economic Geology, 88, 1402-1418.

Barnes, S-J., Maier, W.D. and Ashwal, L.D., 2004. Platinum-group element distribution in the Main Zone and Upper Zone of the Bushveld Complex, South Africa. Chemical Geology, 208, 294-317.

Brügmannn G.E., Naldrett, A.J., Asif, M., Lightfoot, P.C., Gorbachev, N.S., Fedorenko, V.A., 1993. Siderophile and chalcophile metals as tracers of the evolution of the Siberian Trap in the Noril'sk region, Russia. Geochim Cosmochim Acta, 57, 2001–2018.

CGGJC (Co-operative Geological Group of Japan China in the Panxi Region), 1986. Geology of the Panxi region, Sichuan Province, southwest China. Yamaguchi University, Japan. 340 pp.

Greenough, J.D., Owen, J.V., 1992. Platinum-group element geochemistry of continental tholeiites: analysis of the Long Range dyke swarm, Newfoundland, Canada. Chemical Geology, 98, 203–219.

Hack, P.J., Nielsen, R.L., Johnston, A.D., 1994. Experimentally-determined rare-earth element and Y partitioning behaviour between clinopyroxene and basaltic liquids at pressures up to 20 kbar. Chemical Geology, 117, 89–105.

Lightfoot, P.C., Hawkesworth, C.J., Hergt, J., Naldrett, A.J., Gorbachev, N.S., Fedorenko, V.A., Doherty, W., 1994. Chemostratigraphy of Siberian trap lavas, Noril'sk district, Russia: implications for the evolution of flood basalt magmas. In: Lightfoot, P.C., Naldrett, A.J. (Eds.), Proceedings of the Sudbury-Noril'sk Symposium. Ontario Geological Survey, Special Publication 5, 283–312.

Li, C., Naldrett, A.J., 1999. Geology and petrology of the Voisey's Bay intrusion: reaction of olivine with sulfide and silicate liquids. Lithos, 47, 1–31.

Li, C., Maier, W.D., de Waal, S.A., 2001. Magmatic versus PGE deposits: Contrasting genetic controls and exploration implications. South African Journal of Geology, 104, 309-318.

Li, Z.X., Li, X.H., Kinny, P.D., Wang, J., Zhang, S., Zhou, H., 2003. Geochronology of Neoproterozoic syn-rift magmatism in the Yangtze Craton, South China and correlations with other continents: evidence for a mantle superplume that broke up Rodinia. Precambrian Research, 122, 85–109.

Maier, W.D., 2005. Platinum-group element (PGE) deposits and occurrences: mineralization styles, genetic concepts, and exploration criteria. Journal of African Earth Sciences, 41, 165–191.

Maier, W.D., Li, C., De Waal, S.A., 2001. Why are there no major Ni-Cu sulfide deposits in large layered mafic-ultramafic intrusions? The Canadian Mineralogist, 39, 547-556.

McKay, G.A., 1989. Partitioning of rare earth elements between major silicate minerals and basaltic melts. In: Lipin, B.R. and McKay, G.A. (Eds.), Geochemistry and Mineralogy of Rare Earth Elements. Reviews in Mineralogy, Mineralogical Society of America, 21, 45-78.

Munteanu, M., Wilson, A.H., Yao, Y., Jiang, S.Y., Chunnett, G., Luo, Y., Mafurutu, L., Phadagi, R., 2010. A conduit-related genesis of the Lengshuiqing intrusive assemblage (Sichuan, SW China). Journal of Volcanology and Geothermal Research, 189, 118-130

Shellnutt, J.G., Zhou, M.-F., Zellmer, G., 2009. Formation of peralkaline A-type granitoids: insights from the Permian Fe–Ti-oxide bearing Baima Igneous Complex (China). Chemical Geology, 259, 204–217.

Sun, S.-S., McDonough, W.F., 1989. Chemical and isotopic systematics of oceanic basalts: implications for mantle composition and processes. In: Saunders, A.D., Norry, M.J. (Eds.), Magmatism in the Ocean Basins. Geological Society Special Publication no. 42, 313–345.

Tao, Y., Li, C., Hu, R., Ripley, E.M., Du, A., Zhong, H., 2007a. Petrogenesis of the Pt–Pd mineralized Jinbaoshan ultramafic intrusion in the Permian Emeishan Large Igneous

Province, SW China. Contrib. Mineral. Petrol. 153, 321–337.

Tao, Y., Li, C., Song, X.Y., Ripley, E.M., Du, A., Zhong, H., 2007b. Mineralogical, petrological, and geochemical studies of the Limahe mafic–ultramatic intrusion and associated Ni–Cu sulfide ores, SW China. Miner. Depos. 43, 849–872.

Wang, C.Y., Zhou, M.-F., 2006. Genesis of the Permian Baimazhai magmatic Ni–Cu–(PGE) sulfide deposit, Yunnan, SW China. Miner. Depos. 41, 771–783.

Wang, C.Y., Zhou, M.-F., Zhao, D.G., 2005. Mineral chemistry of chromite from the Permian Jinbaoshan Pt–Pd-sulphide-bearing ultramafic intrusion in SW China with petrogenetic implications. Lithos 83, 47–66.

Wang, C.Y., Zhou, M.-F., Keays, R.R., 2006. Geochemical constraints on the origin of the Permian Baimazhai mafic-ultramafic intrusion. Contributions to Mineralogy and Petrology, 152, 309–321.

Xiao, L., Xu, Y.G., Mei, H.J., Zheng, Y.F., He, B., Pirajno, F., 2004. Distinct mantle sources of low-Ti and high-Ti basalts from the western Emeishan large igneous province, SW China: implications for plume lithosphere interaction. Earth and Planetary Science Letters, 228, 525–546.

Xu, Y.G., Chung, S.L., Jahn, B.M., Wu, G.Y., 2001. Petrologic and geochemical constraints on the petrogenesis of Permian–Triassic Emeishan flood basalts in southwestern China. Lithos, 58, 145–168.

Xu, Y.G., He, B., Chung, S.L., Menzies, M.A., Frey, F.A., 2004. The geologic, geochemical and geophysical consequences of plume involvement in the Emeishan flood basalt province. Geology, 32, 917–920.

Yao, Y., Viljoen, M.J., Viljoen, R.P., Wilson, A.H., Zhong, H., Liu, B.G., Ying, H.L., Tu, G.Z., Luo, Y.N., 2001. Geological characteristics of PGE-bearing layered intrusions in southwest Sichuan Province, China. Information Circular no. 358. Economic Geology Research Institute, Hugh Allsopp Laboratory, University of the Witwatersrand, Johannesburg, 21 pp.

Zhao, J.H., Zhou, M.-F., 2007a. Geochemistry of Neoproterozoic mafic intrusions in the Panzhihua district (Sichuan Province, SW China): implications for subduction-related metasomatism in the upper mantle. Precambrian Research, 152, 27–47.

Zhao, J.H., Zhou, M.-F., 2007b. Neoproterozoic adakitic plutons and arc magmatism along the western margin of the Yangtze Block, South China. Journal of Geology, 115, 675–689.

Zhong, H., Zhu, W.G., 2006. Geochronology of layered mafic intrusionsfrom the Panxi area in the Emeishan large igneous province, SW China. Mineralium Deposita, 41, 599–606.

Zhou, M.F., Malpas, J., Song, X., Robinson, P.T., Sun, M., Kennedy, A.K., Lesher, C.M., Keays, R.R., 2002a. A temporal link between the Emeishan large igneous province (SW China) and the end-Guadalupian mass extinction. Earth and Planetary Science Letters, 196, 113–122.

Zhou, M.-F., Yan, D.P., Kennedy, A.K., Li, Y.Q., Ding, J., 2002b. SHRIMP zircon geochronological and geochemical evidence for Neoproterozoic arc-related magmatism along the western margin of the Yangtze Block, South China. Earth and Planetary Science Letters, 196, 51–67.

Zhou, M.-F., Robinson, P.T., Lesher, C.M., Keays, R.R., Zhang, C.-J., Malpas, J., 2005. Geochemistry, petrogenesis, and metallogenesis of the Panzhihua gabbroic layered intrusion and associated Fe-Ti-V-oxide deposits, Sichuan Province, SW China. Journal of Petrology, 46, 2253–2280.

Zhou, M.F., Arndt, N.T., Malpas, J., Wang, C.Y., Kennedy, A.K., 2008. Two magma series and associated ore deposit types in the Permian Emeishan large igneous province, SW China. Lithos, 103, 352–368.

Zhu, D., Xu, Y.G., Luo, T.Y., Song, X.Y., Tao, Y., Huang, Z.L., Zhu, C.M., Cai, E.Z., 2007. Conduit of the Emeishan basalts: the Zhubu mafic-ultramafic intrusion in the Yuanmou area of Yunnan Province, China (in Chinese, with English Abstract). Acta Mineralogica Sinica, 27, 273-280.